Large-Scale Vertical Motions and MJO Convective Onset

Scott W. Powell and Robert A. Houze, Jr., *University of Washington, Seattle, WA*

1. Introduction

- Powell and Houze (2013) document three MJO events during DYNAMO/AMIE.
- Ground-based radar and rawinsonde data from AMF2 detected a 3–7 day build-up of convection and humidity prior to MJO convective onset at Gan.
- On this poster, we first show that such spatially limited datasets contain ~30-day variability in convective behavior and dynamic/thermodynamic tropospheric structure that is representative of the same on the large-scale.
- A mechanism linking upper-tropospheric velocity potential anomalies, observed to circumnavigate the tropics during DYNAMO/AMIE (Gottschalck et al. 2013), to MJO convective onset is then proposed using the ground-based radar and large-scale forcing derived from rawinsonde data (Johnson et al. 2015).

2. Large-Scale Convective/Environmental Variability

Large-Scale Behavior of Convection as Seen by TRMM PR

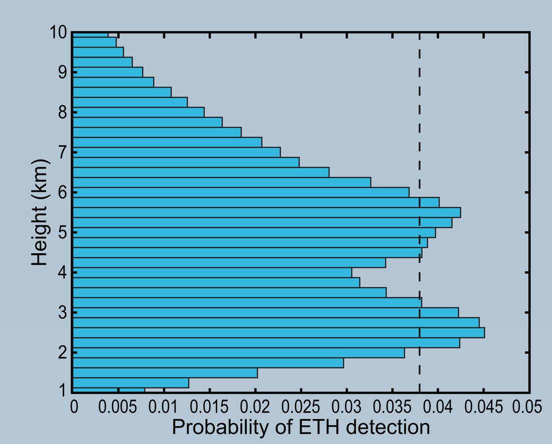

Probability distribution of detecting a 20 dBZ echo top height (ETH) for all convective echoes between 9°S, 9°N, 60°E, and 100°E from 1 October 2011 – 15 January 2012.

Conclusions

- Evolution of convective depth as seen by S-PolKa consistent with that on the large-scale.
- Two modes of convection observed.
- Transition from shallower mode (congestus) to deeper mode (deep convection) occurred over 2–8 day period prior to MJO onset.
- Areal coverage of congestus increases sharply for 2–4 days followed by a decrease when areal coverage of deep convection rapidly increases at MJO onset.
- Results are consistent with Powell and Houze (2013), Ruppert and Johnson (2015).

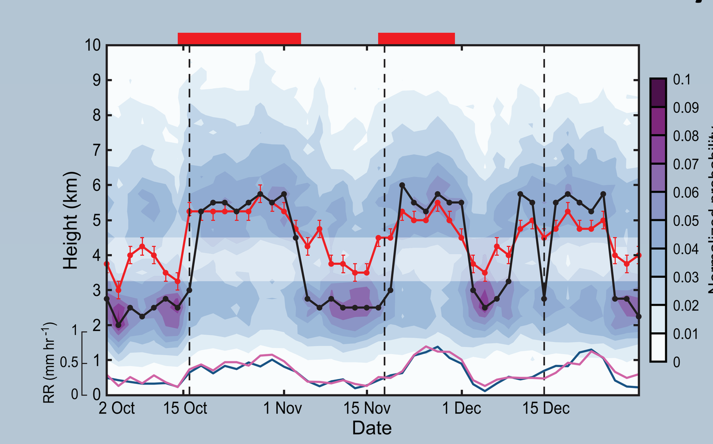

Time series of the normalized probability of 20 dBZ echo top height for a domain enclosed by 9°S, 9°N, 60°E, and 100°E and smoothed to two-day intervals during the interval 1 October – 31 December.

Black line = Mode of ETH distribution
Red line = Median of ETH distribution
Red error bars = 95% confidence bound of red line
Dashed black lines = Date of first MCS observed by S-PolKa during each MJO convective event
White box separates modes of convective depth (see top left).
Blue (*purple*) *line* at bottom: Time series of 3B42[1] (2A25) domain-averaged rain rate smoothed to 2-day intervals.

[1]Domain-averaged 3B42 time series of rain rate correlates with S-Pol derived rain rate at ρ = 0.56 with 95% confidence interval 0.25 ≤ ρ ≤ 0.77. 3B42 and 2A25 time series correlate at ρ = 0.91 (0.76 ≤ ρ ≤ 0.97).

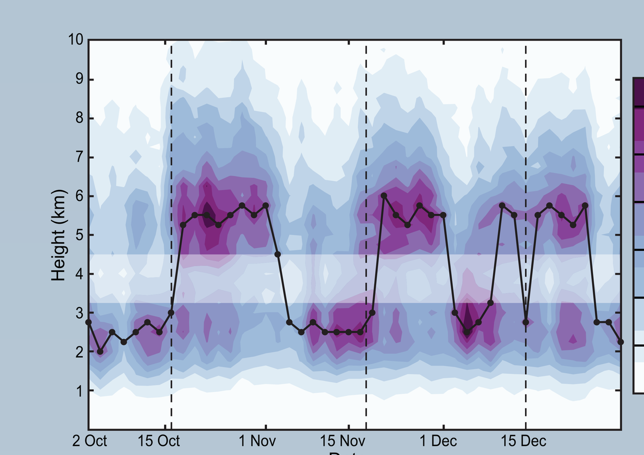

Time series, smoothed to two-day intervals, of the histogram of detected 20 dBZ echo top heights between 9°S – 9°N and 60° – 100°E.

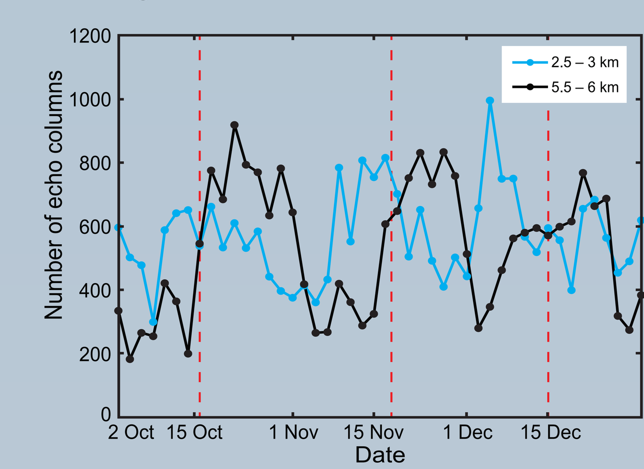

Line plot, in two-day intervals, of the total echo tops detected at heights 2.5 – 3 km (blue) and 5.5 – 6 km (black)

Time Series of Large-Scale Zonal Wind, Temperature, and Humidity in ERA-Interim (60–100°E; 9°N–9°S)

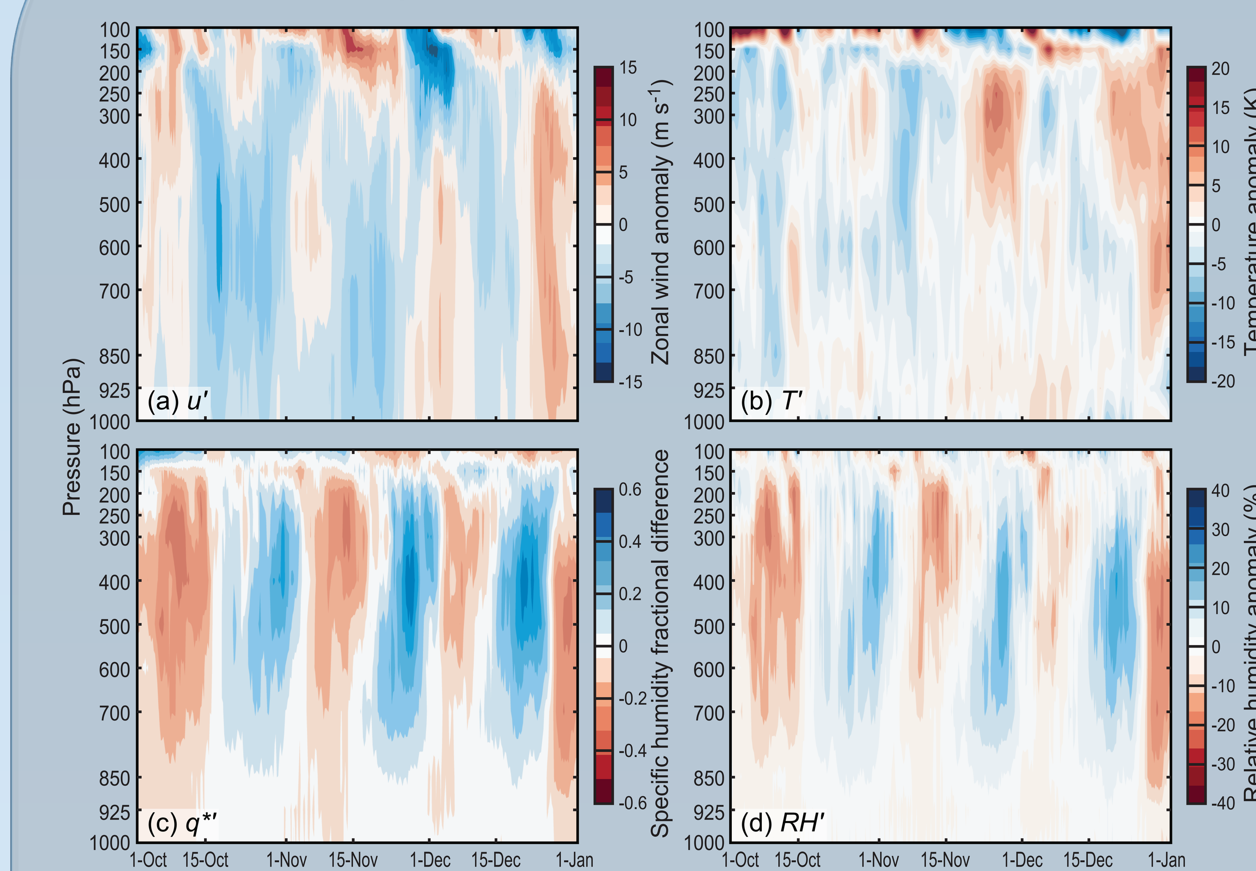

	68–78°E; 3°N–3°S	60–100°E; 9°N–9°S
u'	0.85 ≤ 0.87 ≤ 0.89	0.55 ≤ 0.61 ≤ 0.66
T'	0.68 ≤ 0.71 ≤ 0.73	0.52 ≤ 0.56 ≤ 0.59
$q^{*\prime}$	0.80 ≤ 0.81 ≤ 0.82	0.61 ≤ 0.64 ≤ 0.66

Left: Pearson correlation coefficients ρ (in center of each inequality expression) and 95% confidence intervals between time series of u', T', and $q^{*\prime}$ as derived by Gan rawinsonde data and by ERA-I. Columns are labeled by the domain used to composite ERA-I output.

3. Circumnavigating Signals of Velocity Potential and Vertical Velocity

TRMM 3B42 Precipitation | **150 hPa Velocity Potential Anomaly (χ_{150}')** | **300 hPa Omega Anomaly (ω_{300}')**

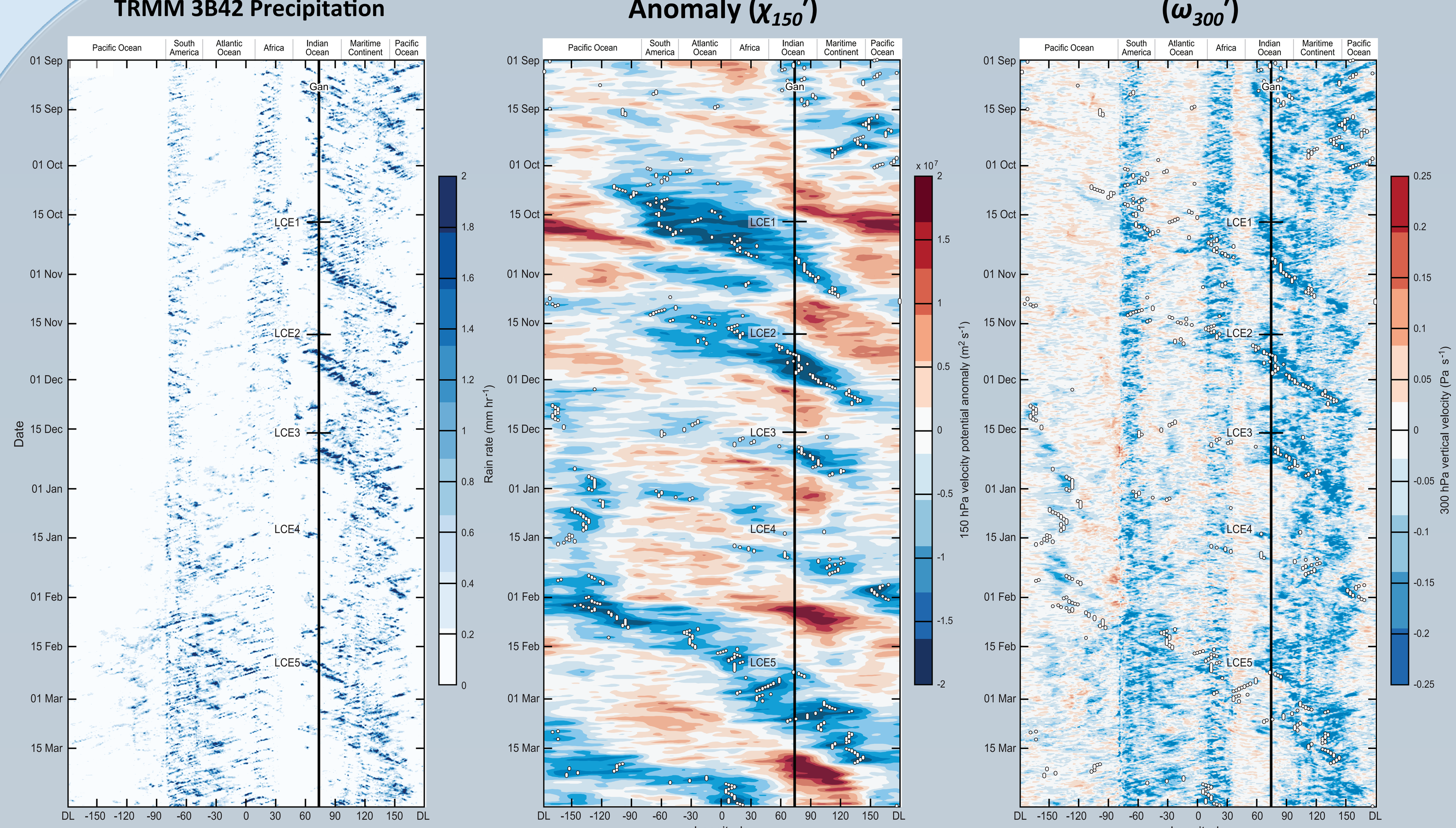

<u>Hovmöllers</u> *(left):* All composited between 3°N and 3°S. White dots represent longitude where χ_{150}' is a minimum at each date/time.

<u>Hovmöllers of Filtered ω_{300}'</u> (*bottom row, left*): ω_{300} is filtered using a Gaussian Fourier filter. The small filter reduces all components of ω_{300} with zonal wavenumber > 6 to 10% of their original magnitude. The large filter does the same with components larger than zonal wavenumber 1.5. White dots represent χ_{150}' filtered the same way as ω_{300}' in each plot.

<u>Mean Longitude-Height Structures</u> (*bottom row, right*): a) Using small filter. b) Using large filter. Both are composited about the longitude of the minimum in unfiltered χ_{150}' during suppressed periods at Gan.

ω_{300}' Small Filter | **ω_{300}' Large Filter**

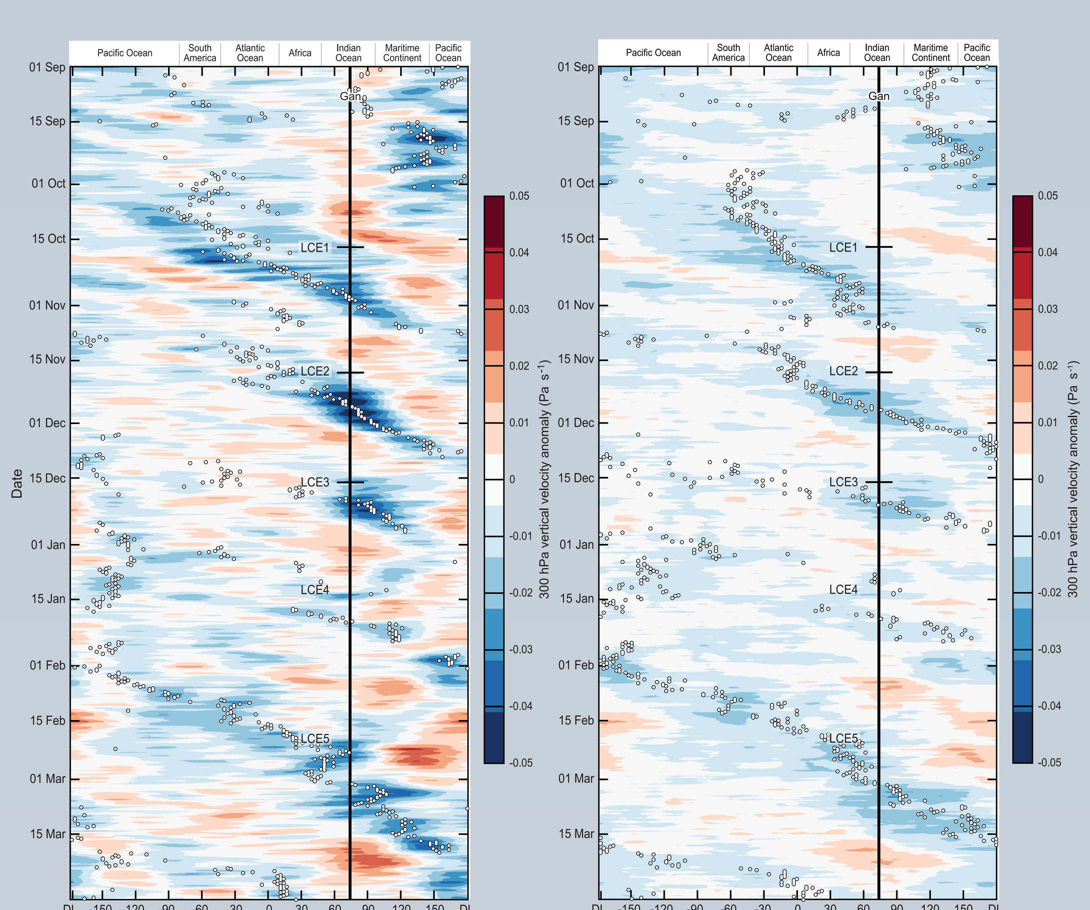

ω' | **u'**

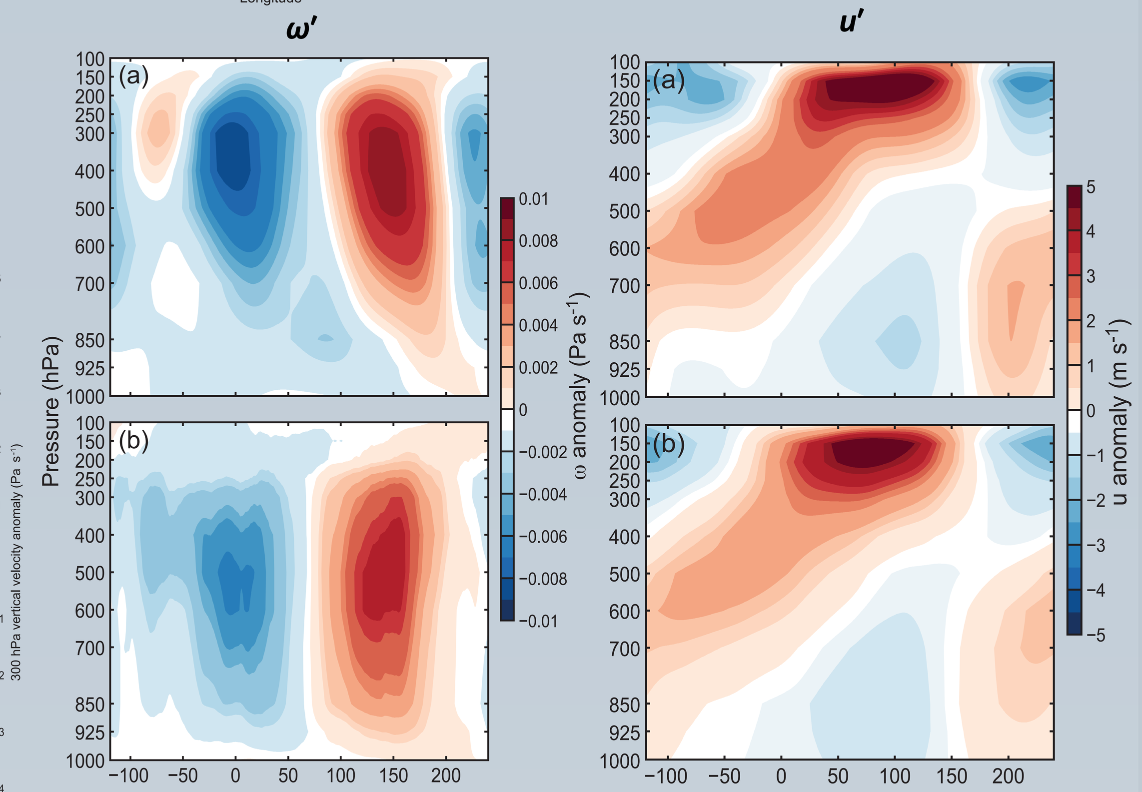

- Clear circumnavigating dry signals of χ_{150}' and low-wavenumber ω_{300}' are detected. They are associated with a wavenumber 1 structure of zonal wind.
- The associated vertical velocity response is consistent with mass continuity.
- Smaller scale (higher zonal wavenumber than 1.5) features may be important for determining exact dates of MJO convective onset.

4. State of the Large-Scale Environment during Shallow to Deep Transition

Brief background: We classified 6-hour blocks prior to MJO convective onset as “Cg”, “transition”, or “Cb” periods. During “Cg” periods, congestus mode convection (echo tops 3–7 km) observed by S-PolKa near Gan did not grow into deep cumulonimbi (tops > 9 km). During “Cb” periods, > 26% of congestus clouds grew. During transition periods, some percentage between. Similar to Kumar et al. (2014).

Right: Circles mark times/dates belonging to each period described above. The two “X” marks for each category correspond to the median date/time of occurrence for each period prior to the two MJO onsets used.

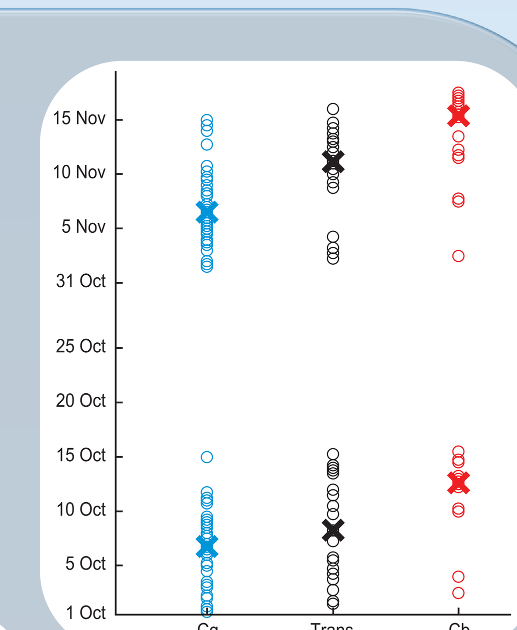

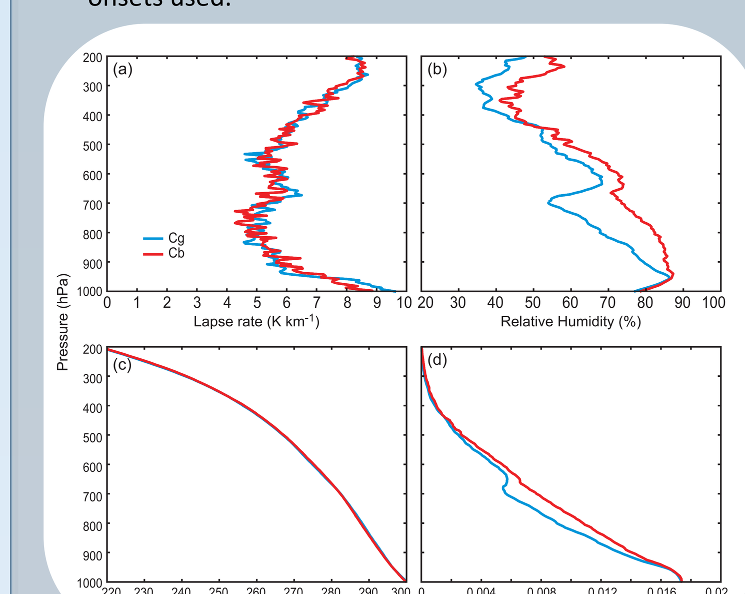

Left: Mean profiles in 6-h prior to “Cg” and “Cb” periods, derived from AMIE rawinsonde data, of lapse rate, relative humidity (RH), temperature, and specific humidity.

RH increases between Cg period and Cb period. Furthermore, changes in RH dominated by changed in specific humidity.

Supports prior studies (i.e. Derbyshire et al. 2004; Wang and Sobel 2012) showing sensitivity of deep convection to low- and mid-tropospheric humidity.

Right: Profiles, derived from CSU large-scale forcing (Johnson et al. 2015), of *ω*, Q_1, Q_2, horizontal, vertical, and total advection, moisture tendency, and $Q_1 - Q_2$.
Purple -> “Cg” period
Black -> “Transition”
Red -> “Cb” period

$$Q_1 - Q_2 = Q_R - L_v \frac{\partial}{\partial p}\left(\overline{\omega' h'}\right)$$

h = moist static energy,
Q_R = radiative heating

$$\frac{\partial q}{\partial t} = \mathrm{v}_h \cdot \nabla q + \omega \frac{\partial q}{\partial p} + Q_2$$

Moistening occurs during transition period. Likely caused by eddy flux divergence of moisture in congestus clouds.

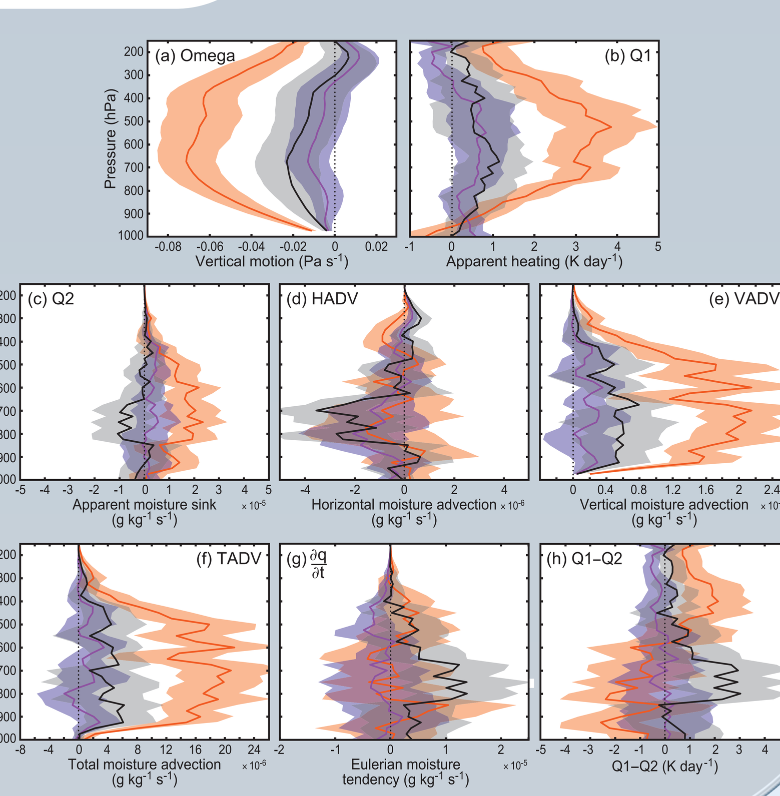

5. Reduction in Subsidence Promotes Moist Convection

Left: Difference in using ω_{300}' with large filter between median dates/times of transition periods and “Cg” periods. As zonal wavenumber 1 feature propagates eastward, it contributes to a reduction in subsidence.

Center: Difference in adiabatic and radiative heating caused by the reduction in subsidence. Radiative cooling reduced as humidity increases, but not enough to compensate for reduction in adiabatic warming.

Right: Fraction of total positive moistening during Cb period that can be attributed to reduction of subsidence. 25–50% of moistening at 300–500 hPa can be explained by reduction of large-scale subsidence.

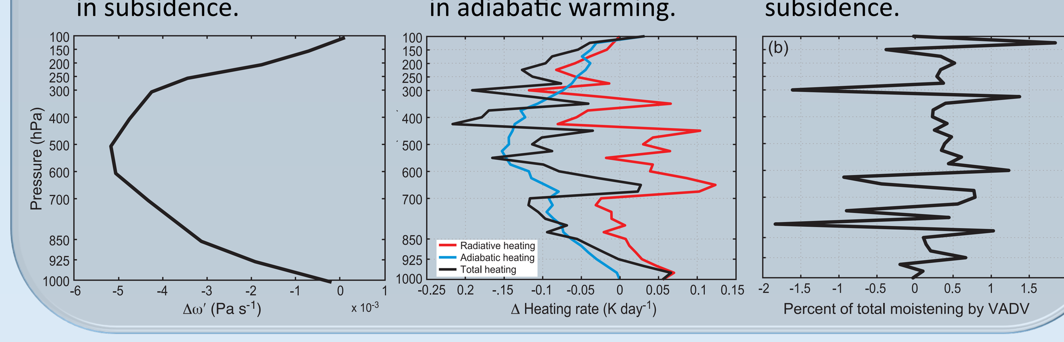

6. Conclusions

- Anomalies of zonal wind, most easily detectable by its large signal near 150–250 hPa, and vertical velocity exist near the equator as a dry wavenumber 1 structure.
- As the upward branch of the zonal wind/vertical velocity structure approaches the Indian Ocean, large-scale subsidence is reduced. As a result, large-scale mean adiabatic heating and radiative cooling are reduced at most levels.
- Reduction in adiabatic heating exceeds reduction in radiative cooling. Moist convection is promoted in the lower troposphere during a 3–7 day long transition period.
- Humidification of the low-troposphere allows deep convection to develop.
- Lessened subsidence enhances upper-tropospheric moistening, allowing deep convection to develop rapidly into mesoscale convective systems.

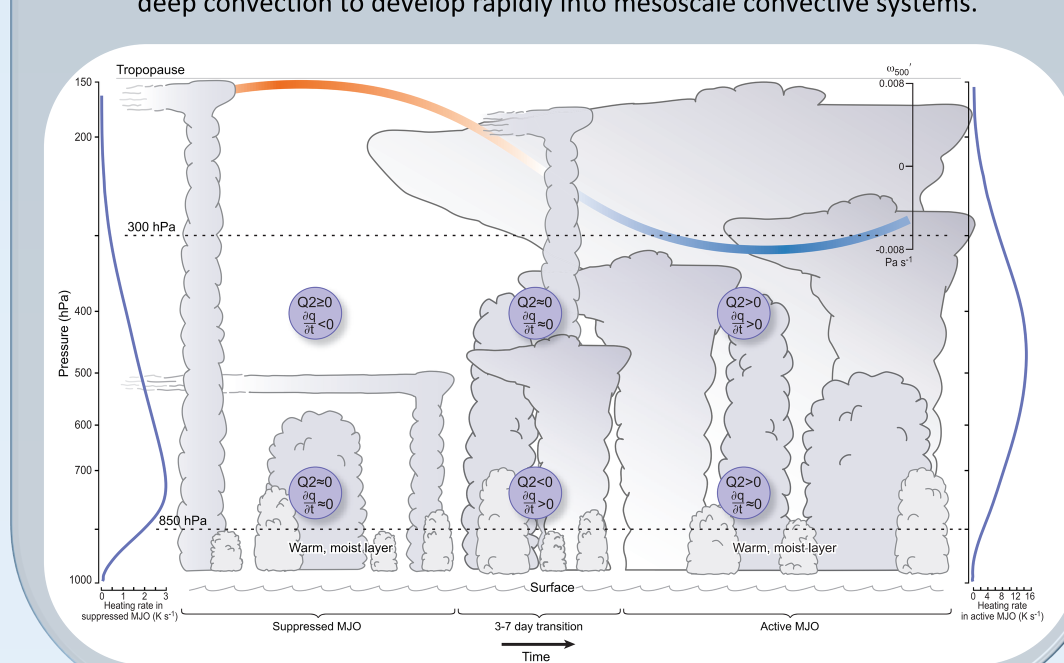

Creation of this poster was supported by DOE grant DE-SC0008452.